Twenty-Seventh Symposium (International) on Combustion/The Combustion Institute, 1998/pp. 2767–2773

EXPERIMENTAL ESTIMATION OF THERMAL EXPANSION AND VORTICITY DISTRIBUTION IN A BUOYANT DIFFUSION FLAME

X. C. ZHOU AND JAYAVANT P. GORE
Thermal Sciences and Propulsion Center
School of Mechanical Engineering
Purdue University
W. Lafayette, IN 47907-1003, USA

The flow induced by buoyant diffusion flames results from thermal expansion caused by heat release and vorticity generated because of density gradients in the flame. The thermal expansion source induces a potential velocity field, and the vorticity induces a solenoidal velocity field. Baum and McCaffrey's technique for the calculation of fire-induced flow field requires specifications of thermal expansion and vorticity source terms. We estimate the thermal expansion using the laminar flamelet method in conjunction with measurements of major gas species concentrations. Mixture fractions are calculated based on the major species concentration data, and gradients of mixture fraction are obtained from the curve fits to the radial profiles of mixture fractions. The temperature, density, and mass diffusivity of the gases are determined using laminar flamelet state relationships from OPPDIF simulations of a natural gas/air diffusion flame. These quantities are needed for estimating the source term for thermal expansion. The mean velocity field is measured using particle imaging velocimetry. The mean vorticity is obtained by differentiating this field using a finite difference. Near the burner surface, the vorticity components based on the axial and radial velocity gradients are approximately equal. A few centimeters from the burner surface, the component involving the axial velocity becomes dominant. We have computed the fire-induced flow field using the method of Baum and McCaffrey in conjunction with the present source term measurements. The results of these computations agree reasonably well with experimental data.

Introduction

A buoyant diffusion flame involves a "natural balance" between many complicated processes, including fluid mechanical, chemical, and heat transfer phenomena and their interaction [1]. As an important factor, many researchers have studied air entrainment of buoyant diffusion flames, as we summarized in Ref. [2]. Many empirical entrainment correlations have been obtained in these studies. However, as identified by Baum and McCaffrey [3], these are suitable only for the conditions of the corresponding investigation. Only computations of the fire-induced flow field from basic equations can provide a more general method. In one such approach [3], decomposing the flow into its irrotational and incompressible components makes the governing equations linear. The irrotational flow is caused by thermal expansion because of chemical energy release. The incompressible flow is induced by vorticity generated by density gradients. In Baum and McCaffrey [3], the source terms of these two component flows, that is, the volumetric heat release rate and vorticity distribution, were evaluated by analyzing the correlations of flame structure by McCaffrey [4]. In Zhou et al. [2], we compared the measured entrainment velocities with predictions of this method extended to a pool fire significantly above a floor [5]. We observed qualitative agreement between measurements and predictions. However, large quantitative differences existed. An ad hoc adjustment of the radial extent of the source terms (determined by the 1/e point in the velocity profile) resulted in a substantial improvement.

Motivated by this, we obtained experimental estimates of the thermal expansion and vorticity source terms in the present study. We mapped the mixture fraction field based on measurements of major gas species concentrations. The source of the velocity potential was evaluated from the mixture fraction distributions and the laminar flamelet concept [6]. The state relationships were obtained from calculations of one-dimensional flat flames using the OPPDIF code [7].

The entrainment flow field is dominated by the incompressible flow caused by the vorticity [3]. In an inviscid flow away from walls, vorticity is generated by density gradients. The gravitational center of the fluid element does not coincide with its geometrical center, through which the pressure acts. Hence, gravitational and pressure forces are not aligned with each other and rotate the fluid element, creating vorticity. As the largest density gradient is at the flame sheet, this region corresponds to a layer

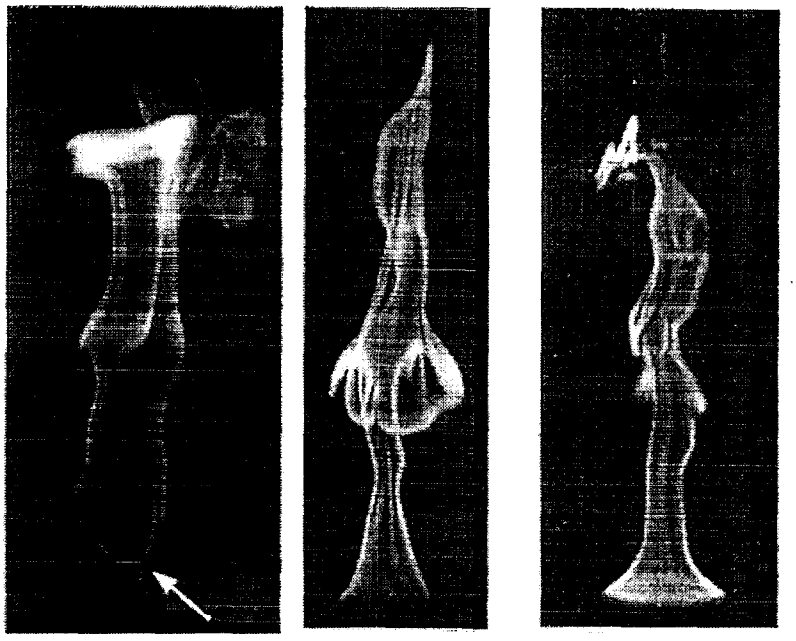

(a) natural gas, tube burner (b) natural gas, diffuser burner (c) toluene pool fire

FIG. 1. Instantaneous shapes of a 7.1-cm buoyant diffusion flame (taken with f = 4.0 and speed = 1/250 s).

of intense vorticity generation. To estimate the vorticity field, we measured the velocity field both inside and outside the flame with a particle-imaging velocimetry (PIV) system. We estimated the vorticity from the mean velocity field using the finite difference method.

The irrotational flow and incompressible components were computed using the measured sources in conjunction with the methods discussed in Refs. [4] and [5]. We compared the resulting fire-induced flow field with measurements.

Experimental Method

Unbiased measurements of velocity using PIV require seeding of fuel and air streams with particles. Therefore, gaseous flames must be studied as surrogates of accidental liquid and solid fires. Honeycombs and porous ceramics used in previous gas-fueled straight burners cause severe obstruction of the seed flow at velocities required for simulating pool fires. A straight tube burner does not provide flame attachment analogous to that of liquid fires (see Figs. 1a and 1c). The gas flame over a diffuser burner with a seven degree expansion angle provides a better surrogate of the liquid pool fire (Figs. 1b and 1c). A fuel flow rate of 102.9 mL/s gives a fire Froude number of 0.109, identical to that of the toluene fire of Fig. 1c studied in Ref. [8]. Utility natural gas containing 92.2% CH_4, 3.3% C_2H_4, 3.9% N_2, and 0.67% CO_2 is used as fuel. The gas has an effective molecular weight of 15.76 and a stoichiometric mass ratio of 0.055.

A gas chromatograph with a calibrated thermal conductivity detector was used for the measurement of N_2, O_2, H_2, CH_4, CO, CO_2, C_2H_4, and C_2H_2 volume fractions. A quartz microprobe with an opening of 200 μm at the tip was used to obtain dry-based samples of the local gas species. The mole fraction of H_2O was estimated using a C-H atom balance. The resulting data were used to calculate the local mixture fraction (carbon based) within an uncertainty of 10%.

The velocity field was measured with a PIV system, schematically very similar to the system used in Zhou et al. [2], except that a II-10 Nd:YAG laser was used to provide dual pulses at a frequency of 10 Hz. The separation between the pulses was adjusted between 50 and 250 μs. To reduce the effect of flame luminosity, the camera shutter was opened for only the duration of the laser pulses. A filter of 1-nm width around 532 nm was also used. Only a few laboratories are applying the PIV technique to buoyant flows [2,9]. In the present study, 100 images acquired over a 2-hour period showed a range of phases in the pulsation cycle, but a bias of the mean data toward a particular phase was not observed. Agreement between mean velocities from the first 50 and the last 50 images showed that 100 images yield statistically converged data. The uncertainty of the velocity measurement was about 15% except in low-velocity regions near the burner surface, where it can be as large as 25%. Reducing the size of the interrogation box by one-third, reducing the grid spacing by half, or calculating the vorticity using Richardson's extrapolation did not have significant

effects. The velocity field was mapped by moving the burner downward until an axial distance of 35 cm was reached, where the vorticity is less than 10% of the values near the burner.

Theoretical Method

According to the laminar flamelet concept, all scalar properties are functions of mixture fraction at locations away from flame attachment and extinction. Representing the density as a function of mixture fraction only,

$$\frac{\partial \rho}{\partial t} = \frac{d\rho}{dZ}\frac{\partial Z}{\partial t} = \frac{d(1/v)}{dZ}\frac{\partial Z}{\partial t} = -\rho^2 \frac{dv}{dZ}\frac{\partial Z}{\partial t} \quad (1)$$

Similarly,

$$\nabla \rho = -\rho^2 \frac{dv}{dZ} \nabla Z \quad (2)$$

The conservation of mass and mixture fraction equations for the pool fire are

$$\frac{\partial \rho}{\partial t} + \rho \nabla \cdot \vec{V} + \vec{V} \cdot \nabla \rho = 0 \quad (3)$$

$$\rho \frac{\partial Z}{\partial t} + \rho \vec{V} \cdot \nabla Z = \nabla \cdot (\rho D \nabla Z) \quad (4)$$

Substituting equation 1 and equation 2 into equation 3 gives

$$-\rho^2 \frac{dv}{dZ}\frac{\partial \rho}{\partial t} + \rho \nabla \cdot \vec{V} - \rho^2 \frac{dv}{dZ} \vec{V} \cdot \nabla Z = 0 \quad (5)$$

$\rho dv/dZ \times (4) + (5)$ yields the governing equation of the irrotational flow [6]:

$$\nabla \cdot \vec{V} = \frac{dv}{dZ} \nabla \cdot (\rho D \nabla Z) \quad (6)$$

$\nabla \cdot \vec{V}$ represents the local volumetric expansion of the fluid element. Because this flow component is free of vorticity, the velocity can be defined as the gradient of a potential function Φ, and the left-hand side of equation 6 can be written as the second derivative of Φ. $dv/dZ(\nabla \cdot \rho D \nabla Z)$ is the source term of thermal expansion specified experimentally. dv/dZ and ρD are expressed as a function of Z using OPPDIF calculations [7].

From the state equation $P = \rho RT$ and with the assumption of constant thermodynamic pressure,

$$\frac{\partial T}{\partial t} = -\frac{P}{R}\frac{1}{\rho^2}\frac{\partial \rho}{\partial t} \text{ and } \nabla T = -\frac{P}{R}\frac{1}{\rho^2}\nabla \rho \quad (7)$$

With the assumption of unity Lewis number, the energy equation can be written as

$$\rho C_p \frac{\partial T}{\partial t} + \rho C_p \vec{V} \cdot \nabla T = \nabla \cdot \rho D \nabla T + \dot{Q}''' \quad (8)$$

Substituting equation 7 for T in equation 8 and adding to $TC_p \times$ equation 3 yields

$$\nabla \cdot \vec{V} = \frac{\dot{Q}'''}{C_p \rho_\infty T_\infty} + \frac{\nabla \cdot \rho D \nabla T}{C_p \rho_\infty T_\infty} \quad (9)$$

where it is assumed that the product of density and temperature is constant. A comparison of equation 9 with equation 6 explains the physical origins of expansion flow. The first term on the right-hand side of equation 9 is the volumetric heat release rate, and the second term is the thermal conduction rate. The measurements of species concentrations are used to estimate the local thermodynamic temperatures, and the contributions of thermal conduction to the expansion source term are estimated using finite difference.

The solenoidal component of the fire-induced flow field is related to the vorticity distribution in the fire as

$$\nabla \times \vec{V} = \omega_p \quad (10)$$

Vorticity is generated only by a density gradient away from a solid boundary [3]. Because derivative and averaging of velocity field are interchangeable, the mean vorticity distribution is estimated by taking curl of the mean velocity field with a central difference formula.

Results and Discussion

Figure 2 shows measurements of mixture fraction plotted as a function of radial distance for three axial locations relatively close to the burner surface. Analytical curves are fitted to the mixture fraction data using the least squares method to obtain continuous derivatives. Gaussian profiles have been used in the past [3] to represent the distributions of scalar properties in the plume region of pool fires. Near the burner surface, radial profiles of the mixture fraction are flat in the center region because of initial conditions. Therefore a four-parameter logistic function $f(r) = (a - d)/(1 + \exp(b(r - c)) + d)$ provides a better approximation. At 1.5 cm from the burner surface, the Gaussian and the logistic-function profiles both provide reasonable fits to the data. Measurements of radial distributions of mixture fraction were obtained for 14 stations within the flame, up to an axial distance of 30 cm. Farther downstream, the Gaussian profile provides a better approximation to the mixture fraction distribution. The present measurements of mole fractions support the use of laminar flame state relationships.

Figure 3 shows the source of the velocity potential and net thermal conduction plotted as a function of

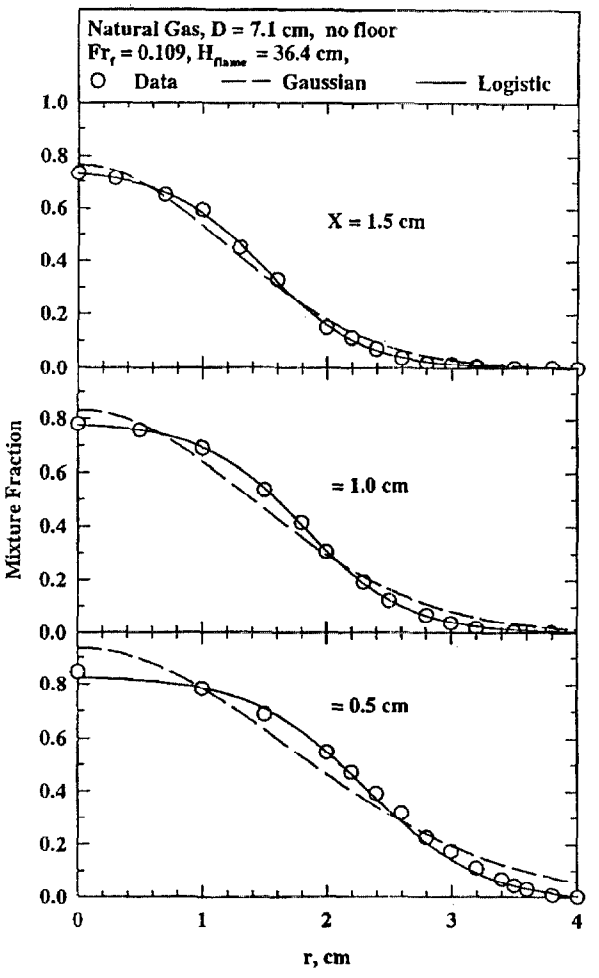

FIG. 2. Radial distribution of mixture fraction at $x = 0.5$, 1, and 1.5 cm of a 7.1-cm natural gas flame at $Fr_f = 0.109$.

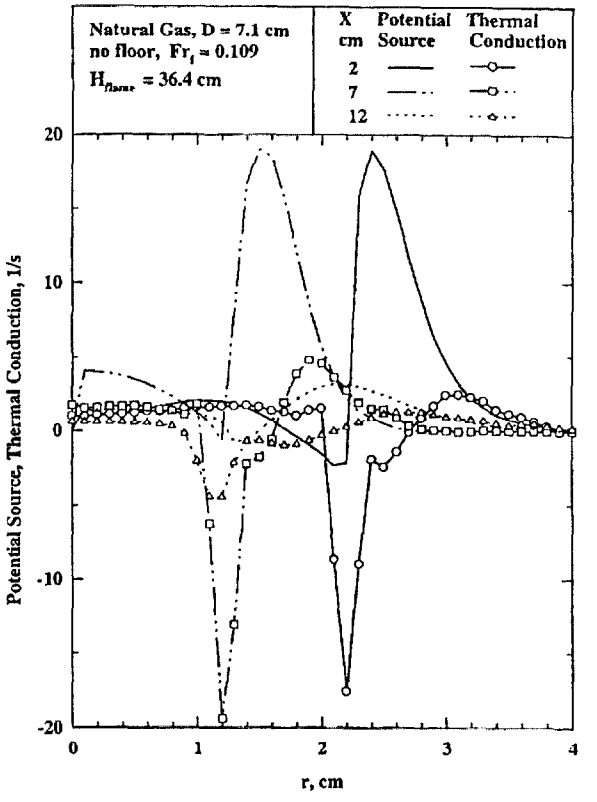

FIG. 3. Velocity potential source as a function of radial distance at $x = 0.5$, 2.0, 7.0, 10.0, and 12.0 cm of a 7.1-cm natural gas flame at $Fr_f = 0.109$.

radial distance for three representative axial locations (2, 7, and 12 cm above the burner). The curves with symbols on them represent thermal conduction, and those without symbols represent the net thermal expansion source term. The peak thermal conduction has comparable magnitude to the peak thermal expansion, and on the inner side of flame sheet, the values of thermal conduction are negative. At $x = 2$ cm, the peak of thermal expansion source term is reached at about $r = 2.4$ cm, and at $x = 7$ cm, it moves to $r = 1.5$ cm. The general features of the radial distribution of the velocity potential are that the source term is close to zero in the region near the axis, followed by a small annular region of negative values and a narrow region of high positive values that terminate to zero in the ambient air. Further downstream ($x \geq 10$ cm), the radial profiles of the velocity potential source term are similar to those at the lower positions, except for smaller values and a considerable broadening of the annulus within which the chemical energy is released. At $x = 12$ cm, the peak average energy release rate is less than 10% of the peak average value at the lower positions. This indicates that the bulk of the heat release is complete in the continuous region (for this flame at an axial distance of about 12 cm), corroborating the findings by Baum and McCaffrey [3].

Radial profiles of the axial velocities at four axial locations are plotted in Fig. 4. Different symbols represent different sets of measurements. Collapsing data from different measurements to one line shows the level of repeatability of the measurements. The bottom panel shows the radial profile of the axial velocities at an axial distance of $x = 1$ cm. Because the buoyancy is the strongest in the flame sheet region, and the flame sheet is close to the burner edge near the burner surface, the profile has a saddle shape. At $x = 2$ cm, the axial velocity at the centerline increases to 40 cm/s from 9 cm/s at $x = 1$ cm. The radial profile of axial velocities still has a saddle shape. At $x = 4$ cm, the axial velocity at the centerline reaches 120 cm/s. Near the centerline, the radial profile of the axial velocities is rather flat. The top panel shows the axial velocities at $x = 6$ cm plotted as a function of radial distance. At the centerline, the axial velocity reaches 160 cm/s.

Figure 5 shows estimates of radial profiles of vorticity at four axial stations, obtained by approximating spatial derivative of velocity with central finite difference analyses of mean velocity data. Since the

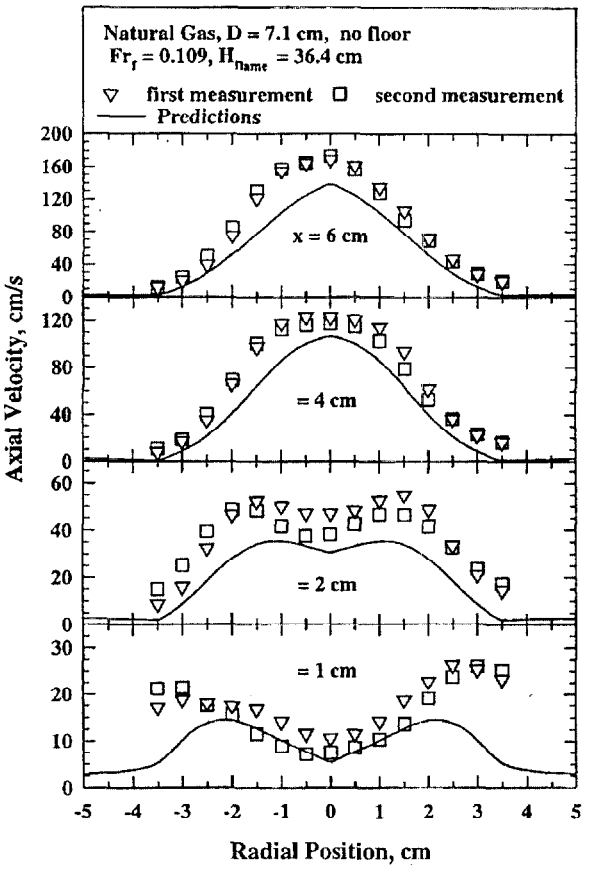

FIG. 4. Axial velocities as a function of radial distance for four stations of a 7.1-cm natural gas flame at Fr_f = 0.109.

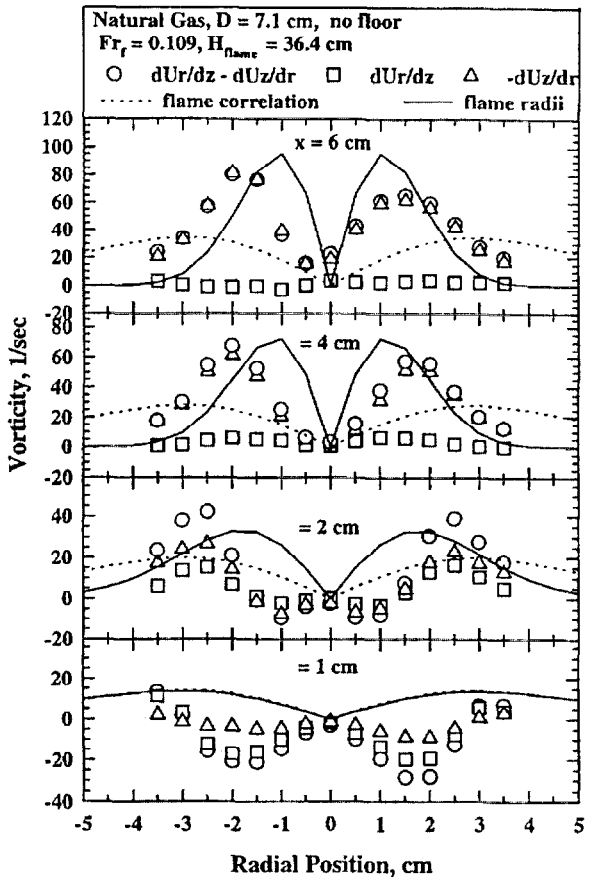

FIG. 5. Vorticity as a function of radial distance at four stations of a 7.1-cm natural gas flame at Fr_f = 0.109.

curl of potential velocity vanishes, the curl of the velocity is equal to the curl of the incompressible component. The triangle symbols represent the negative of the radial gradient of axial velocity, and the square symbols represent the axial gradient of radial velocity. The circle symbols show the total vorticity. Near the burner surface, the two components of the vorticity are of comparable magnitude; however, the component involving radial velocity decreases with increasing axial distance, and the component involving the axial velocity increases rapidly with increasing axial distance. At x = 4 cm, the vorticity component involving the radial gradient of axial velocity is much larger than that involving the axial gradient of radial velocity and dominates the total vorticity. Examination of the velocity vector field shows that this results from the fact that the velocities are mainly in the vertical direction except near the burner surface where large inward radial velocities exist. The dotted lines in Fig. 5 show predicted vorticity values with flame radii obtained from heat flux analysis of McCaffrey's correlations [3], and the solid line shows the vorticity distribution with the ad hoc assumption regarding the 1/e position of the velocity profile made in Zhou et al. [2]. Near the flame base, the two estimates are close to each other, and both have positive values, while the measured values are negative. At downstream locations, the magnitude of the vorticity estimated based on the assumption that is made in Ref. [2] agrees better with the measurements. However, the locations of peak values are different from the locations of the maximum measured vorticity. The vorticity values estimated from McCaffrey's correlations are too low inside and near the flame sheet but too high in the outer region.

The fire-induced flow field, which is a superposition of the incompressible flow and the irrotational flow, is dominated by the vorticity-driven irrotational flow. The results of the computations are compared with the measured velocities in Fig. 4, where the solid lines represent the radial profiles of the axial velocities computed based on the experimental source terms. The agreement between the predictions and the measurements is excellent. The predictions are not only close to the data in absolute value, but also catch the saddle shape of the radial distribution of axial velocities at locations close to the burner surface. This agreement supports the present method of estimating the source term.

Figure 6 shows the comparison between the predicted radial velocities and measurements at r = 3.5

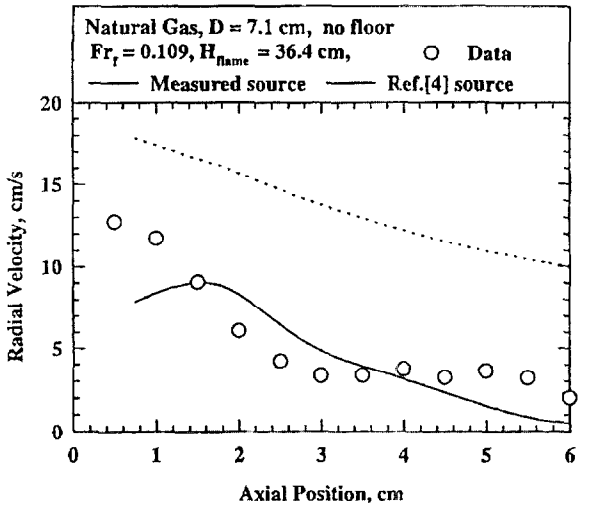

FIG. 6. Comparison between measurements of radial velocities at $r = 3.5$ cm of a 7.1-cm natural gas flame at $Fr_f = 0.109$, with predictions based on different methods to evaluate the source terms of the governing equations.

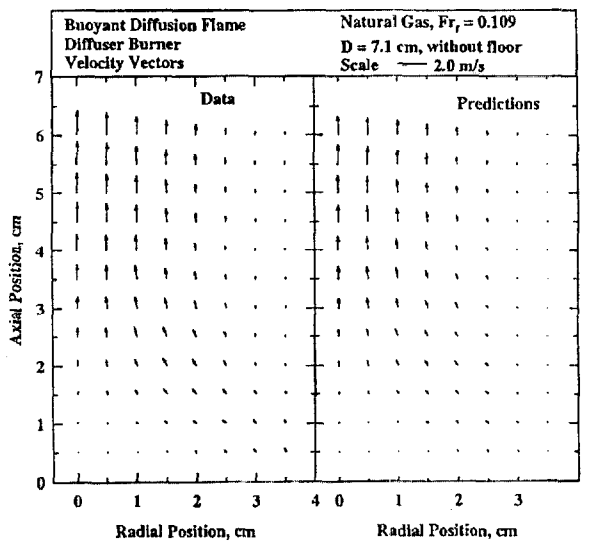

FIG. 7. Measurements and predictions of velocity vectors in a 7.1-cm natural gas fire with $Fr_f = 0.109$.

cm, plotted as a function of axial distance. The circle symbols represent the measured entrainment velocity. The solid line represents the predicted radial velocities based on the measured source obtained in this study. The dashed line shows the predicted radial velocities with source terms estimated from the flame structure correlations, as in Ref. [3]. It is shown clearly that the predictions based on the present measured source terms agree much better with measured entrainment velocities.

Figure 7 shows velocity vectors within the fire based on measurements and predictions. The maximum velocities are approximately 2 m/s, and the minimum velocities are at least a factor of 20 lower than this. Both the measurements and predictions show a conical low-velocity region near the fuel surface. An inflow of air from near the burner edge that follows the visible flame shapes in Fig. 1b and c is observed. This flow moves diagonally inward, reacts, and accelerates, establishing a high-velocity of cylindrical region near the axis. In addition to the radial velocities, a flow of air parallel to the flame axis is also established. There is agreement in all the qualitative features of the measured and predicted flow fields.

Conclusions

1. Estimation of velocity potential source distribution inside the flame is feasible based on the measurement of major gas species concentrations.
2. Estimation of vorticity distribution is feasible based on PIV measurements of the mean velocity field. Near the burner surface, the vorticity components based on the axial and radial velocity gradients are of approximately equal magnitude. However, within a few centimeters from the burner surface, the component involving the axial velocity becomes dominant.
3. With realistic estimates of velocity potential distribution and vorticity distribution, the fire-induced flow field can be predicted accurately by solving the separate governing equations for the incompressible flow and the irrotational flow, following the methodology of Baum and coworkers [2,3,5].
4. The fire-induced flow is dominated by the incompressible flow caused by vorticity generated in the flame sheet region.

Acknowledgments

The research was supported by Center for Fire Research, Building and Fire Research Laboratory, National Institute of Standards and Technology under Grant No. 60NANB6D0118 with Dr. Howard R. Baum serving as NIST Scientific Officer.

REFERENCES

1. Tieszen, S. R., Nicolette, V. F., Gritzo, L. A., Holen, J. K., Murray, D., and Moya, J. L., SANDIA report SAND96-2607, UC-722.
2. Zhou, X. C., Gore, J. P., and Baum, H. R., in *Twenty-Sixth Symposium (International) on Combustion*, The Combustion Institute, Pittsburgh, 1996, pp. 1453–1459.
3. Baum, H. R. and McCaffrey, B. J., in *Fire Safety Science—Proceedings of the Second International Symposium*, Tokyo, Japan, 1988, pp. 129–148.

4. McCaffrey, B. J., *Combust. Flame* 52:149–167 (1983).
5. Zhou, X. C., Gore, J. P., and Baum. H. R., *Joint Meeting of the Central States/Western States*, The Combustion Institute, San Antonio, Texas, April 23–26, 1995.
6. Baum, H. R., Rehm, R. G., and Gore, J. P., *Twenty-Third Symposium (International) on Combustion*, The Combustion Institute, 1990.
7. Lutz, A. E. and Kee, R. J., *OPPDIF: A Fortran Program for Computing Opposed Flow Diffusion Flames*, SANDIA report SAND 96-8243, UC1409.
8. Zhou, X. C. and Gore, J. P., NIST-GCR-97-706, National Institute of Standards and Technology, 1997.
9. Cetegen, B. M., *Combust. Sci. Technol.* 123:377–387 (1997).

COMMENTS

Michael A. Delichatsios, Renewable Resources Associates, USA. What would the effects of flow fluctuations be on your experimental date and analysis? Also, is it not a circular attempt to predict entrainment rates using local values, which imply that entrainment is known?

Author's Reply. Although we have used a steady-state version of the analysis, if transient source terms for vorticity and thermal expansion are available, flow fluctuations can be computed with transient version of the analysis. However, to evaluate the expansion source term based on the mean mixture fraction field, it has to be assumed that the product of density and diffusivity is a constant and that dv/dZ and $\nabla^2 Z$ are statistically independent. The linearization afforded by the analysis allows accurate evaluation of the mean vorticity source term based on the mean velocity field because the average of the curl is the curl of the average. Both these assumptions introduce an error in the calculations, prompting the present investigation.

The input provided to the analysis is in the form of source term distributions only. The boundary conditions are obtained from asymptotic analysis with a point source of heat release. Therefore, the attempt is not circular but allows an evaluation of the analysis with realistic source terms and boundary conditions.

•

James Quintiere, University of Maryland, USA. Please comment on the accuracy of your approach in determining entrainment by point velocity measurements on the calculated velocity field by the potential flow/velocity technique compared to global measurements of entrainment by mass balance techniques. The latter appears to have less source of potential error.

Author's Reply. The components, such as collection hoods, used in global measurement techniques affect the fire-induced velocity field and lead to inconsistent definitions of air entrainment. The resulting correlations are good only for the specific experimental techniques and conditions. For example, Beyler found that measured air-entrainment rates using a sampling hood can be different by a factor of 2 depending on where combustion products exhaust [1]. With the present technique, the air-entrainment rates defined in a consistent manner can be measured within 15% [2,3].

REFERENCES

1. Beyler, C. L., Ph.D. thesis, Harvard University, Cambridge, MA, 1983.
2. Zhou, X. C., Gore, J. P., and Baum, H. R., in *Twenty-Sixth Symposium (International) on Combustion*, The Combustion Institute, Pittsburgh, 1996, pp. 1453–1459.
3. Joulain, P., in *Twenty-Seventh Symposium (International) on Combustion*, The Combustion Institute, Pittsburgh, 1998, pp. 2691–2704.

•

Kuldeep Prasad, Naval Research Laboratory, USA. Can you discuss the effect of boundary conditions, side wall, and burner wall on the entrainment and velocity vectors? The velocity vectors due to heat release alone indicate a source located at a height of 5 cm along the centerline. This contradicts numerical results that show that most heat release occurs close to the fuel–air interface just above the burner surface.

Author's Reply. Along the centerline, radial velocities in both component flows are zero due to axisymmetry; hence, the radial gradient of the potential function is zero, and the stream function is a constant. On the outer boundaries, the values of the potential function and the stream function are asymptotic values computed using a point source of heat release (Ref. [2] in answer to previous comment). Our data show that from the burner surface to a height of about 10 cm, the potential source term resulting from the heat release has a peak value near the mean visible flame boundary as shown in Fig. 3. The velocity vectors resulting from the expansion source term diverge from a location at a height of 5 cm along the centerline, but this should not be interpreted as indicating that there is a source of heat release at that location. Instead, Fig. 3 should be consulted to determine the location of the source of heat release.